Acta Materialia xxx (2018) xxx-xxx

Contents lists available at ScienceDirect

Acta Materialia

journal homepage: www.elsevier.com

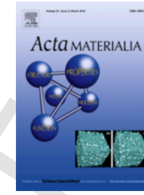

UNCORRECTED PROOF

Full length article

Micromechanical modeling of non-linear stress-strain behavior of polycrystalline microcracked materials under tension

Giovanni Bruno[a, b], Mark Kachanov[c, d], Igor Sevostianov[e, *], Amit Shyam[f]

[a] BAM, Bundesanstalt für Materialforschung und -prüfung, Unter den Eichen 87, D-12205, Berlin, Germany
[b] University of Potsdam, Institute of Physics and Astronomy, Karl-Liebknecht-Str. 24-25, 14476, Potsdam, Germany
[c] Department of Mechanical Engineering, Tufts University, Medford, MA, 02155, USA
[d] R.E.Alexeev Nizhny Novgorod Technical University, Nizhny Novgorod, 603155, Russia
[e] Department of Mechanical and Aerospace Engineering, New Mexico State University, Las Cruces, NM, 88003, USA
[f] Oak Ridge National Laboratory, 1 Bethel Valley Road, Oak Ridge, 37831-6069, TN, USA

ARTICLE INFO

Article history:
Received 12 June 2018
Received in revised form 13 September 2018
Accepted 12 October 2018
Available online xxx

Keywords:
Nonlinearity
Stress-strain relations
Hysteresis
Tension
Ceramics
Rocks
Polycrystals

ABSTRACT

The stress-strain behavior of microcracked polycrystalline materials (such as ceramics or rocks) under conditions of tensile, displacement-controlled, loading is discussed. Micromechanical explanation and modeling of the basic features, such as non-linearity and hysteresis in stress-strain curves, is developed, with stable microcrack propagation and "roughness" of intergranular cracks playing critical roles. Experiments involving complex loading histories ~~were~~ done on large- and medium grain size β-eucryptite ceramic. The model is shown to reproduce the basic features of the observed stress-strain curves.

© 2018.

1. Introduction

We consider the behavior of brittle polycrystalline materials (such as ceramics or rocks) that have certain amount of pre-existing intergranular microcracking, under tensile, displacement-controlled, loading and unloading. Typically, these existing microcracks stem from cooling from high temperatures, *e.g.* after sintering in ceramics [33], and are due to the thermal expansion contrast, either between different phases or between different orientations of crystallites of the same phase. Fig. 1 shows typical microcrack geometries in ceramics and rocks; it is seen that microcracks have complex shapes that follow grain boundaries and other weak surfaces in the microstructure (that depend on the crystallography of the grains or domains [1–3]). Furthermore, the microcrack faces possess certain "roughness" that is dictated by orientation of the grains and presence of other phases along the crack propagation path. During tensile loading, stable microcrack growth starts on most favorably oriented microcracks (normal to the loading direction) ~~and~~ that are sufficiently large. This results in non-linearity of the stress-strain curve. The non-linearity has been shown to increase with loading (Fig. 2). Note that, although microcrack propagation under displacement-controlled conditions is generally stable, yet another possible factor contributing to the stability is that, having to follow grain boundaries or other weak surfaces, microcracks may run into geometries where the energy release rates are substantially reduced (for example, T-intersections, Fig. 1).

Fig. 2 shows the stress-strain behavior of rocks and ceramics under displacement-controlled tensile loading. Fig. 2a [4] refers to several types of rocks; almost vertical drops indicate formation of extensive microcrack networks within narrow range of applied strain; note that this load-drop does not imply failure. Fig. 2b [5] reproduces the data on cordierite subjected to tensile loading cycles with identical peak stresses; the hysteresis observed in the first cycle (upper loop) almost vanishes in subsequent cycles. Fig. 2c [6] represents the data for β-eucryptite subjected to a full loading-unloading cycle followed by re-loading to a higher load compared to maximum load in the previous cycle.

The following features of the stress-strain curves should be highlighted (Fig. 2):

(A) In the *first* loading, the curve "softens" and becomes non-linear. Upon ~~shifting to~~ unloading, the slope of the curve increases noticeably ("stiffer" response). At full unloading, certain residual

* Corresponding author.
Email address: igor@nmsu.edu (I. Sevostianov)

https://doi.org/10.1016/j.actamat.2018.10.024
1359-6454/ © 2018.

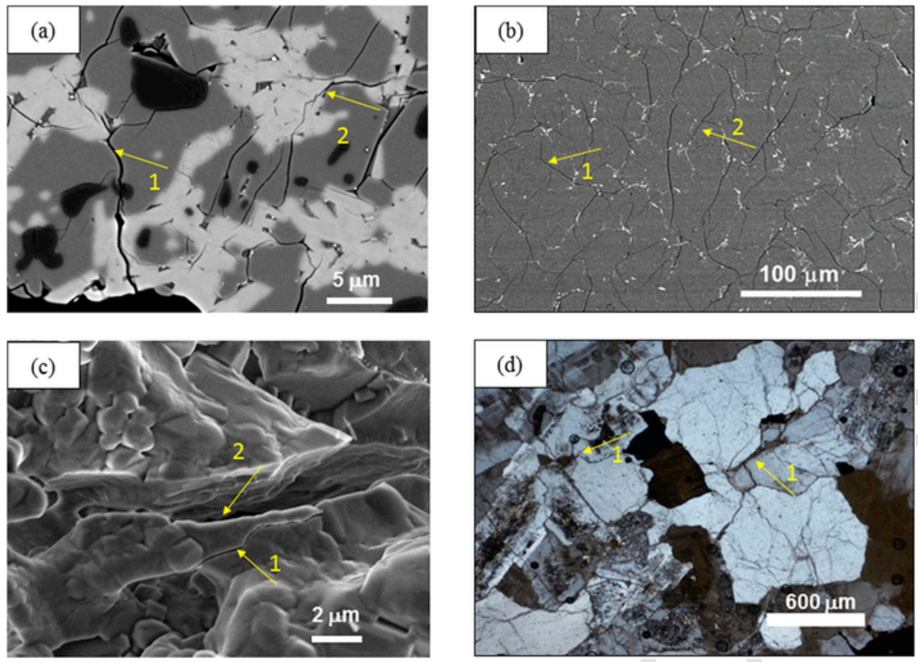

Fig. 1. Typical microstructures of brittle microcracked polycrustalline materials: (a) aluminum titanite; (b) β-eucryptite; (c) cordierite; (d) silesian granite (from Ref. [31]). Arrows (1) indicate locations of cracks following grain boundaries; arrows (2) point to roughness of crack faces.

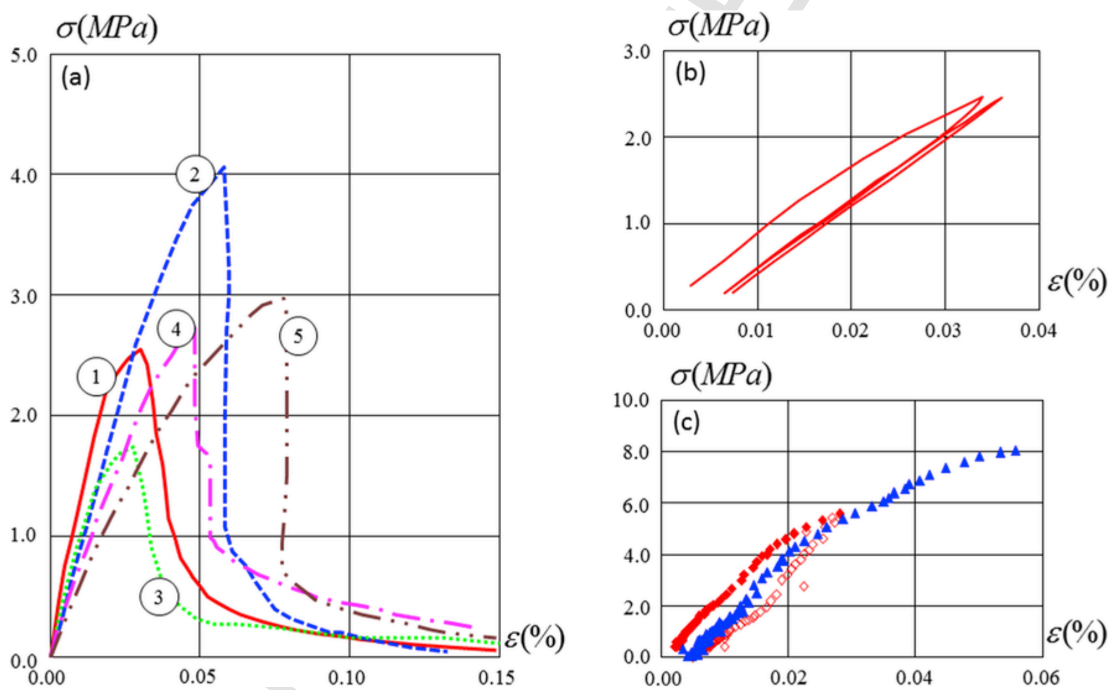

Fig. 2. Stress-strain curves reported for (a) several rocks: 1 – akiyoshi marble, 2- sanjome andesite, 3- kuzu dolomite, 4 – kawazu tuff, 5 – tako sandstone (from Ref. [4]); (b) cordierite (from Ref. [5]); (c) β-eucryptite (from Ref. [6]).

strain remains. The first loading-unloading cycle exhibits substantial hysteresis;

(B) In subsequent cycles, the loading-unloading curves become almost linear (no hysteresis is observed in Fig. 2b) – provided the peak load does not exceed the one in the first cycle;

(C) If the peak load in the next cycle exceeds the one in the previous cycle, the loading curve becomes nonlinear above this point;

In the context of geological materials, some of these features have been observed starting from the 1970's. Hawkes and Mellor [7] conducted tensile tests on Berea sandstone, Indiana limestone, and Barre granite and reported that at low loads the Young's modulus is similar in tension and compression, but decreases in tension at higher loads and increases in compression, up to the stage of incipient failure. Stimpson and Chen [8] proposed a testing technique in which the moduli in both tension and compression can be measured on the same specimen and reported nonlinear behavior under tensile loading of several rocks (halite, potash, granite, and limestone). Okubo and Fukui [4] performed uniaxial tension tests on nine Japanese rocks and observed that the stress-strain curves in tension are non-linear; some of them are shown in Fig. 2a. Heap et al. [32] observed evolution of the elastic moduli of basalt with increasing microcrack density under displacement-controlled loading. They also observed that upon further cycling microcracking only proceeds if the load exceeds the maximum load of all preceding cycles. Young et al. [9] attributed the non-linearity in tension to stable growth of microcracks, as also mentioned in Ref. [10].

In the context of ceramics, Kroupa [11] discussed similar nonlinearities in thermally sprayed ceramic coatings under tension and attributed the decrease of Young's modulus to increase of microcrack density; he suggested a semi-empirical relation for the nonlinearity. Sadowski and Samborski [12] considered nonlinear behavior of porous polycrystalline ceramics in tension and compression, and related the intergranular character of crack propagation to smaller fracture surface energy of grain boundaries. Gao et al. [5] discussed a possible micromechanism of nonlinearity that involves frictional sliding on parts of zigzag cracks induced by tensile loads. More recently, several papers have demonstrated increase in the microcrack density under tensile loading [3,6,10,13]. Cooper et al. [10] made an attempt to model the non-linearity of tensile stress-strain curves; they utilized a modified differential scheme assuming microcrack extension as the main damage mechanism; the microcrack evolution parameters were chosen as linear function of applied strain. They did not provide, however, any micromechanical explanation of the behavior under cyclic loading (increased stiffness at unloading and the resulting hysteresis). Further, they stated that the crack density remains unchanged – and hence continues to contribute to the stress-strain relation – as one switches from loading to unloading. This assumption implies that stiffnesses at both peak loading and onset of unloading are the same, $E = E_{peak}(\varepsilon_{\max})$ - contrary even to the experimental results presented in their paper.

The present work provides micromechanical explanations and modeling of the features (A) – (C) discussed earlier. The quantitative model involves an empirical part that describes the increase of crack density on applied strain, which cannot be derived analytically. The model is validated by the existing experimental data and then verified by new data on β-eucryptite ceramics subjected to cyclic tensile loading.

2. Micromechanical explanation and modeling

We suggest a micromechanical explanation of the features (A)-(C) described above. It is based on two factors: (1) complex crack geometries that follow grain boundaries or weak surfaces, and (2) roughness of crack faces, with roughness profiles getting "mismatched" as cracks propagate, thus impeding the reversal of displacements of crack faces at unloading. The sketch in Fig. 3 illustrates the role of roughness.

The features (A) related to the *first* loading cycle can be explained as follows. The softening in forward loading is due to microcracking; similarly, the feature (C) is related to additional microcracking at loading above the previous peak. The behavior at unloading is related to roughness of crack surfaces. Indeed, in *forward* loading, relative displacements of crack faces comprise both the normal (opening) and the tangential components. If crack propagation occurs, then roughness profiles of crack faces get "mismatched", and this prevents full reversal of the mentioned displacements at unloading. This leads to "stiffer" response at unloading (as compared to the end of loading), to hysteresis, and to consequent residual strain.

In subsequent cycles, the mismatched (due to crack growth) roughness profiles prevent movement of crack faces; the cracks are "stuck" in the positions reached at the peak load. This leads to almost linear stress-strain curves, as described in feature (B).

Remark. The mismatch occurs due to small-scale roughness of crack faces (clearly seen in the exemplary photomicrographs in Fig. 1). When a crack propagates, it experiences not only the normal opening but the *shear* displacement discontinuity as well, so that the rough profiles shift with respect to one another. This causes the mismatch that, upon unloading, prevents full backsliding on the crack. This phenomenon constitutes one of the basic features of the proposed micromechanical model.

Quantitative modeling of stress-strain curves requires a model for the effective elastic properties of a polycrystalline material (treated as homogenized isotropic material) that contains cracks. We use the differential scheme that has been shown to be relatively accurate for cracked solids [14]. This scheme introduces inhomogeneities in increments of concentration, until the final concentration is reached, with homogenization of the background matrix after each increment. Since the increments are infinitesimal, the corresponding increments of the effective constants are found from the dilute limit results. This leads to first-order differential equations for the effective constants as functions of concentration. This scheme, first formulated by Bruggeman [15,16] for the effective dielectric and elastic constants of a matrix with spherical inhomogeneities, was applied to the elastic properties of cracked solids in Refs. [17,18]; for the ellipsoidal inhomogeneities, the equations were given by McLaughlin [19], who solved them explicitly for spherical inhomogeneities; this solution was further analyzed in Refs. [20,21].

In the isotropic case of randomly oriented inhomogeneities, we have two coupled differential equations for the effective bulk and shear moduli. If, however, we are interested in Young's modulus only, then one can construct a simple approximate solution that has satisfactory accuracy if Poisson's ratio of the material prior to loading $\nu_0 < 0.4$ [22]; in the case of circular cracks, it has the form, see the book of Kachanov and Sevostianov [23]:

$$E \approx E_0 e^{-D_0\ \Delta\rho} \tag{1}$$

where $D_0 = -(16/45)\left(1-\nu_0^2\right)\left(10-3\nu_0\right)/\left(2-\nu_0\right)$ and subscript "0" refers to material prior to loading; $\Delta\rho$ denotes the increase of crack density under loading (with respect to the initially microcracked state).

In displacement-controlled loading, the crack density increases as $\rho = \rho(\varepsilon)$. If this dependence is known, formula (1) gives Young's modulus as a function of applied strain, $E = E(\varepsilon)$. In Ref. [10], a linear dependence of the microcrack density on strain has been assumed: $\rho = \rho_0 + B\varepsilon$ (where, ρ_0 is the microcrack density of the material before loading and B is a fitting parameter). This assumption was not given any physical background and was made for sake of simplicity.

Modeling of complex crack geometries. The crack density parameter used in formulas above is defined for ~~the~~ circular (penny shaped) cracks only: $\rho = (1/V)\sum a_k^3$ where a_k is the k-th crack radius and V is the representative volume. It can still be used for flat (planar) cracks of "irregular" in-plane geometries, in the sense that an equivalent set of circular cracks producing the same effect exists [24]. How-

UNCORRECTED PROOF

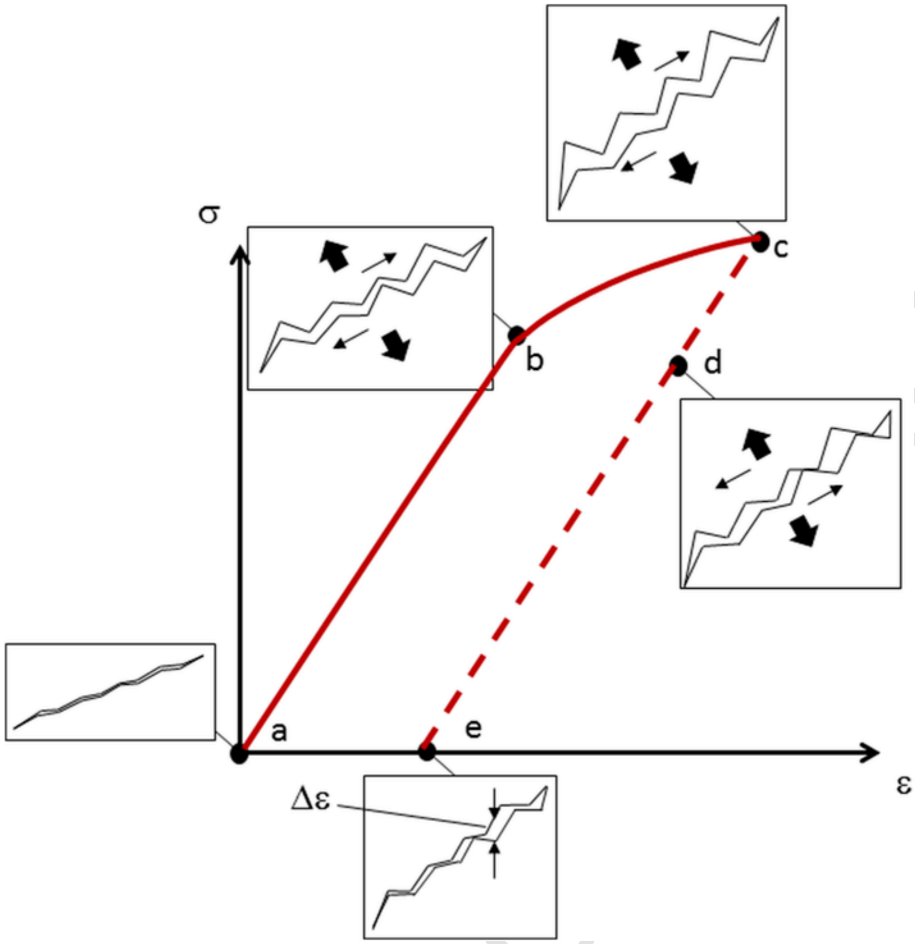

Fig. 3. Sketch illustrating the role of roughness of crack faces. In forward loading, roughness profiles of crack faces get mismatched when nonlinearity starts due to crack propagation (point 2); at unloading (point 4) the faces get "stuck" (their displacement at peak load ~~C~~ is locked).

ever, intergranular cracks are non-flat, and for them not only the crack density parameter is not defined but an equivalent set of circular cracks may exist only for certain geometries [25]. Hence, crack density parameter becomes a "fuzzy" concept: it characterizes crack concentration in the way that may not have immediate geometrical interpretation (while we may regard the microcrack density of penny-shaped cracks as the total volume of the spheres circumscribed over those cracks divided by the volume of the whole specimen). We emphasize this point, we call this "fuzzy" parameter "generalized crack density", denote it by R (rather than ρ for penny-shaped cracks) and proceed as follows:

- We observe that, for the dependence $E = E(\varepsilon)$ to be constructed, the parameter R does not actually need to be geometrically defined; it is its *dependence on applied strain* that is needed;
- We retain the structure of formula (1), with $\rho \rightarrow R$:

$$E \approx E_0 e^{-D_0\ \Delta R} \tag{2}$$

Simulation of stress-strain curves for cordierite and β-eucryptite. The problem reduces to formulating the dependence $\Delta R = \Delta R(\varepsilon)$ where "Δ" refers to the increment of microcrack density (compared to its pre-existing level). We select this dependence as to fit the experimentally observed stress-strain curves. This is achieved by taking

$$\Delta R(\varepsilon) = e^{a\varepsilon^2} - 1 \tag{3}$$

where a is a fitting parameter; for cordierite and β-eucryptite, the value $a = 85$ happens to be the same, and provides the best fit (as discussed in Section 4, parameter a is generally grain size-dependent). The values of E_0 and ν_0 refer to the material prior to loading (they reflect the pre-existing level of microcracking); for cordierite and β-eucryptite, $E_0 = 90\ GPa$, $\nu_0 = 0.20$ and $E_0 = 24\ GPa$, $\nu_0 = 0.28$, respectively (see Cooper et al., ~~2017~~, as well as Bruno et al., ~~2012~~). For both materials, the procedure of extracting ΔR is illustrated in Fig. 4 (a, b) for cordierite and Fig. 4 (c, d) for β-eucryptite. We combined equations (3) and (2) and varying the fitting parameter a to get the best agreement with the experimental data. Fig. 4(a, c) show the best-fit of the experimental data. Fig. 4(b, d) show the extracted dependencies $\Delta R(\varepsilon)$.

Remark. Note that the exponential in formula (3) is a fitting function. While the choice of this function is arbitrary, the exponential character reflects the material behavior: first, at low applied load, cracks oriented normally to the load direction start to propagate slowly, and then crack growth becomes faster and involves a strongly non-linearly increasing number of crack orientations.

UNCORRECTED PROOF

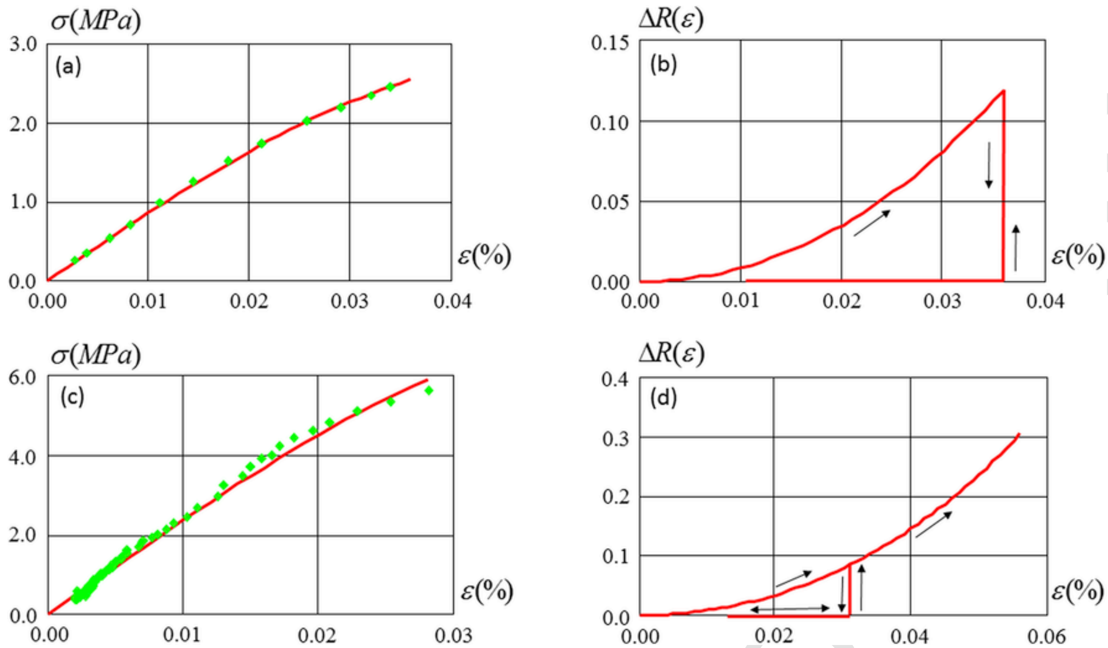

Fig. 4. Procedure of extracting from experimental data: (a) best fit of the stress-strain curve for cordierite [5]; (b) change in generalized crack density as a function of applied strain for corderite; (c) best fit of the stress-strain curve for β-eucriptite [6]; (d) change in generalized crack density as a function of applied strain for beta-eucriptite.

Fig. 5 shows simulation of some of the stress-strain curves shown in Fig. 2. The forward loading curve is simulated by formula $\sigma = E(\varepsilon)(\varepsilon - \varepsilon_{res})$ where $E(\varepsilon)$ is given by Equation (2) and ε_{res} is taken as zero in the first cycle and from the data of Fig. 2b, c in the subsequent cycle. The unloading curve represents linear elastic response corresponding to locking of microcracks (due to roughness) at unloading so that $\sigma = E_0(\varepsilon - \varepsilon_{res})$, ~~i.e.~~ this slope is the same as at the beginning of the forward loading cycle. This feature will be justified and discussed later. The next section demonstrates that the proposed model successfully describes the behavior of ceramics under complex loading histories, as tested by experiments on cyclic loading of microcracked β-eucryptite with large and medium grain sizes.

3. Experiments: cyclic loading with increasing amplitude

The reported experiments were done on beta-eucryptite ceramics specimens. We briefly describe their preparation and microstructure referring to several earlier works for details [6,10,13,26]. The preparation started with a glass precursor consisting of a non-stoichiometric mixture of Li_2O, SiO_2, and Al_2O_3 yielding the chemical formula of the oxide as $LiAlSiO_4$ (β-eucryptite). The glass was poured into large pads that were cerammed using titanium oxide (of less than 5% weight) as nucleating agent. Two materials, with different grain sizes, LGS and MGS (large and medium grain sizes, with average grain sizes of 30 µm and 5 µm respectively) were obtained by the following annealing treatments: 16 h at 1300 °C for LGS and 1h at 1300 °C for MGS. Their typical microstructure is shown in Fig. 6. The MGS ma-

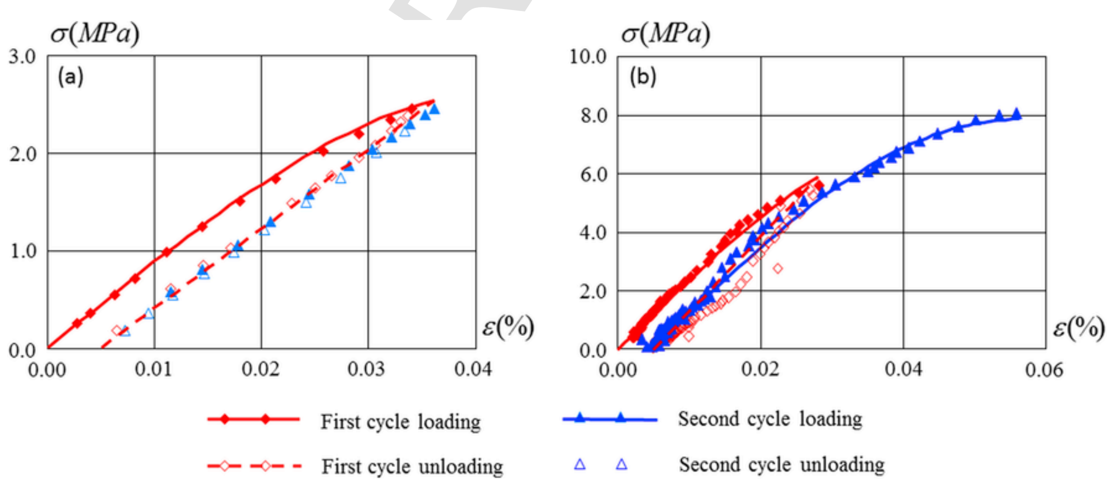

Fig. 5. The first and the second loading-unloading cycles for (a) cordierite and (b) β-eucryptite, as predicted by the model (2) in comparison with the experimental data from Refs. [5,6].

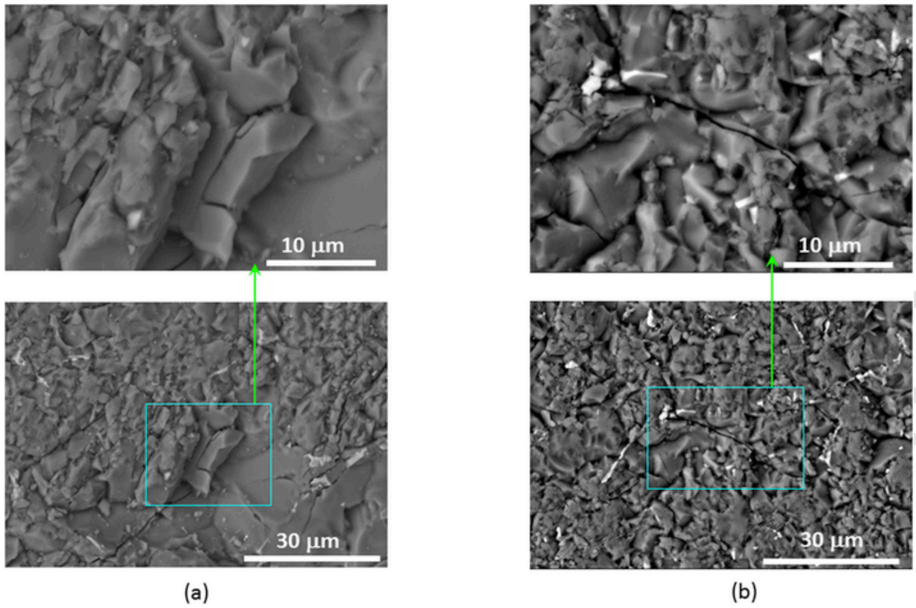

Fig. 6. SEM images of (a) large grain sized (LGS) and (b) medium grain sized (MGS) β-eucryptite.

terial had a moderate level of microcracking, whereas the LGS material had a large density of microcracks (both referring to the conditions prior to loading).

Uniaxial tension experiments were performed on an ORNL in-house built micro tensile rig assembled on an optical bench. An optical microscope was mounted on the rig vertically while the loading direction was horizontal. The optical images were captured periodically (1 Hz acquisition frequency) and analyzed by standard digital image correlation (DIC) techniques, to calculate strain during loading. Details of the procedure, as well as possible errors, have been described in the above-mentioned works. Rectangular specimens were machined and mounted to grips using a thermal forming adhesive. The uniaxial tests were performed at a constant cross-head displacement rate of 1 µm/s for both loading and unloading. Multiple loading and unloading cycles to ~25, 50 and 75% of failure strength were performed. Fig. 7 shows the stress-strain curves for the LGS (a) and MGS (b) specimens. Note that shifting the curves in each cycle to the left by the amount corresponding to the residual strain shows that the Young's modulus of the material remains the same at the beginning of each cycle. Our hypothesis that the stiffness upon unloading matches that at the beginning of forward loading is justified by the experimental data. Physically, it implies that propagating cracks get stuck upon unloading, but other existing cracks continue contributing to the overall compliance to the same amount as for the initially microcracked material.

4. Application of the model to complex loading histories

We apply the developed model to the cyclic tensile loading of beta-eucryptite ceramics (see Section 3) assuming increasing crack density in forward loading and linear elastic unloading corresponding to "locked" microcracks. The results for $\Delta R(\varepsilon)$ are shown in Fig. 8.

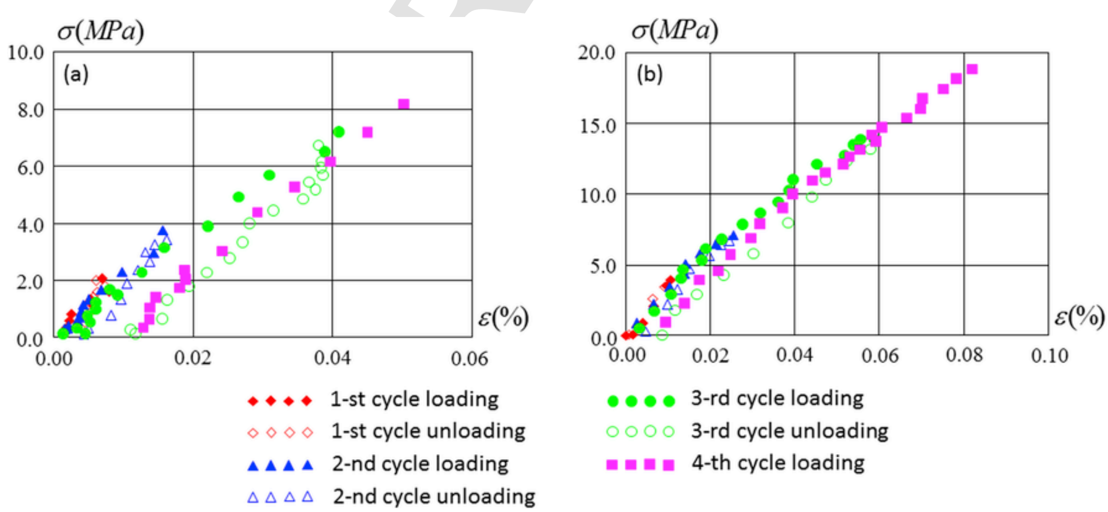

Fig. 7. Stress-strain behavior of (a) LGS and (b) MGS β-eucryptite specimens subjected to cyclic displacement-controlled loading. Solid and empty symbols correspond to loading and unloading, respectively.

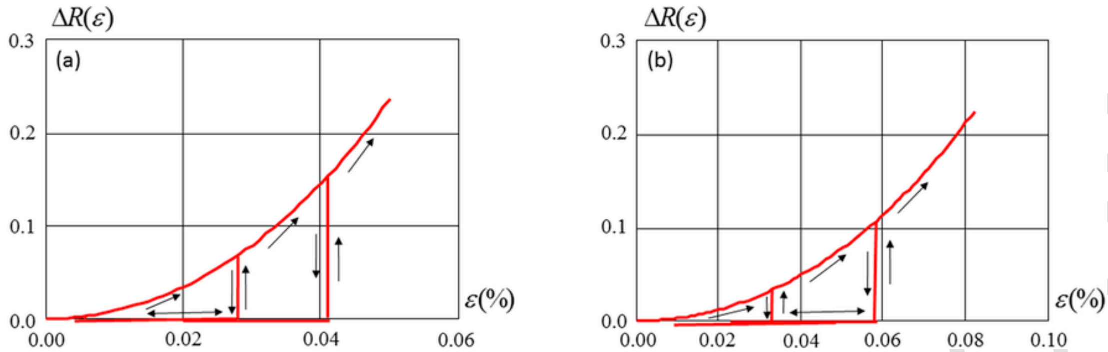

Fig. 8. Changes in generalized crack density during loadings. Vertical lines correspond to locking of crack face displacements during unloading portion of the cycle.

We use the same formula $\Delta R(\varepsilon) = e^{a\varepsilon^2} - 1$ as in Section 2, where the best fit for the LGS and MGS specimens is given by $a = 85$ and $a = 35$ ~~;~~ respectively, indicating grain-size dependence of parameter a.

~~Remark.~~ The value of a is the same for LGS and cordierite (~~Section2~~). In fact, the grain sizes of cordierite and β-eucryptite LGS are nearly the same, while that of MGS is smaller. The dependence of a on grain size is however subject of a separate study.

The values of E_0 are taken as 24 GPa and 34 GPa [10] for the LGS and MGS specimens, respectively – the difference being due to higher pre-existing microcrack density in the LGS specimens. Poisson's ratio is taken as $\nu_0 = 0.28$.

The variation $\Delta R(\varepsilon)$ for the LGS and MGS specimens is shown in Fig. 8. Note that vertical drop to zero for ΔR at unloading reflects locking of cracks resulting in their zero contribution to the overall compliance. Upon reloading, cracks start to contribute to the overall strain only when the previous peak is reached.

Fig. 9 shows the stress-strain behavior during each of the three-and-a-half cycles, for the LGS samples; it compares the simulated curves with the experimental data. Fig. 10 contains similar information for the MGS specimens.

5. Discussion and conclusions

We have proposed a certain micro-mechanism that explains the non-linear behavior of microcracked ceramics under tension (including cyclic loading), and modeled this mechanism quantitatively. The main ideas are that (1) the nonlinearity is related to intergranular (or along weak surfaces) crack propagation and (2) the hysteresis is due to roughness of crack faces that gets "mismatched" due to the propagation and thus impedes backward displacements of crack faces at unloading. The model is shown to be able to reproduce loading and unloading stress-strain curves reported earlier in literature. It is also shown to reproduce the data on complex loading history reported in the present work.

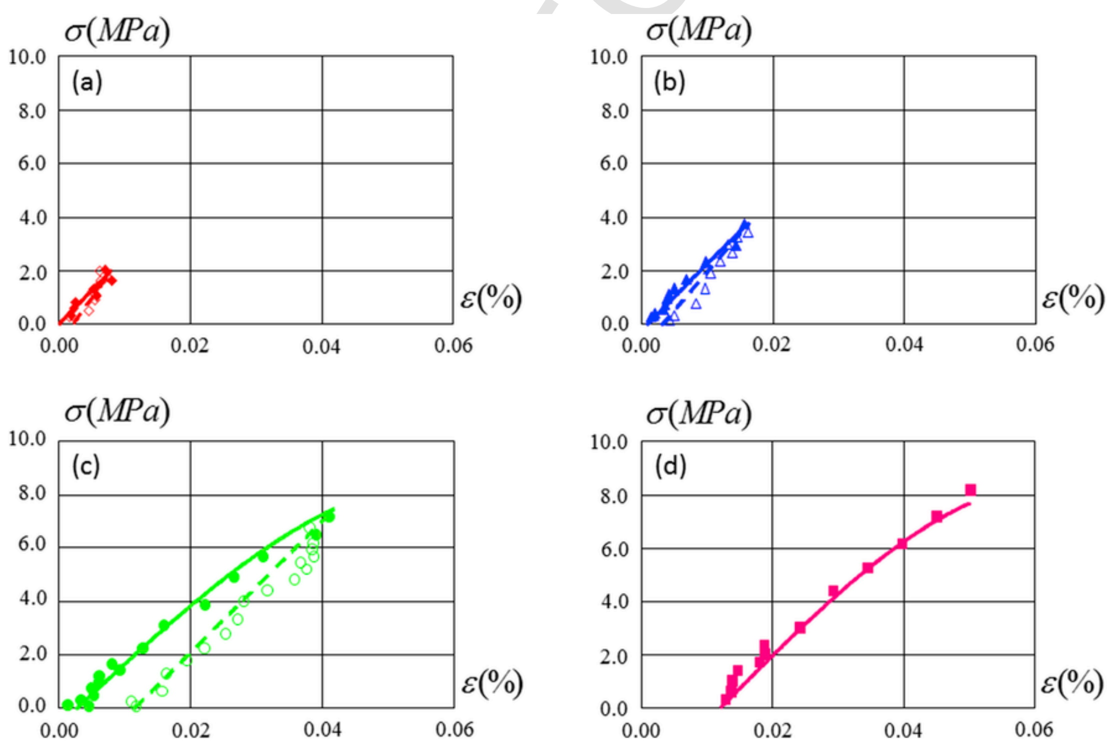

Fig. 9. Comparison of model predictions and experimental data for the three and a half loading-unloading cycles for LGS specimens.

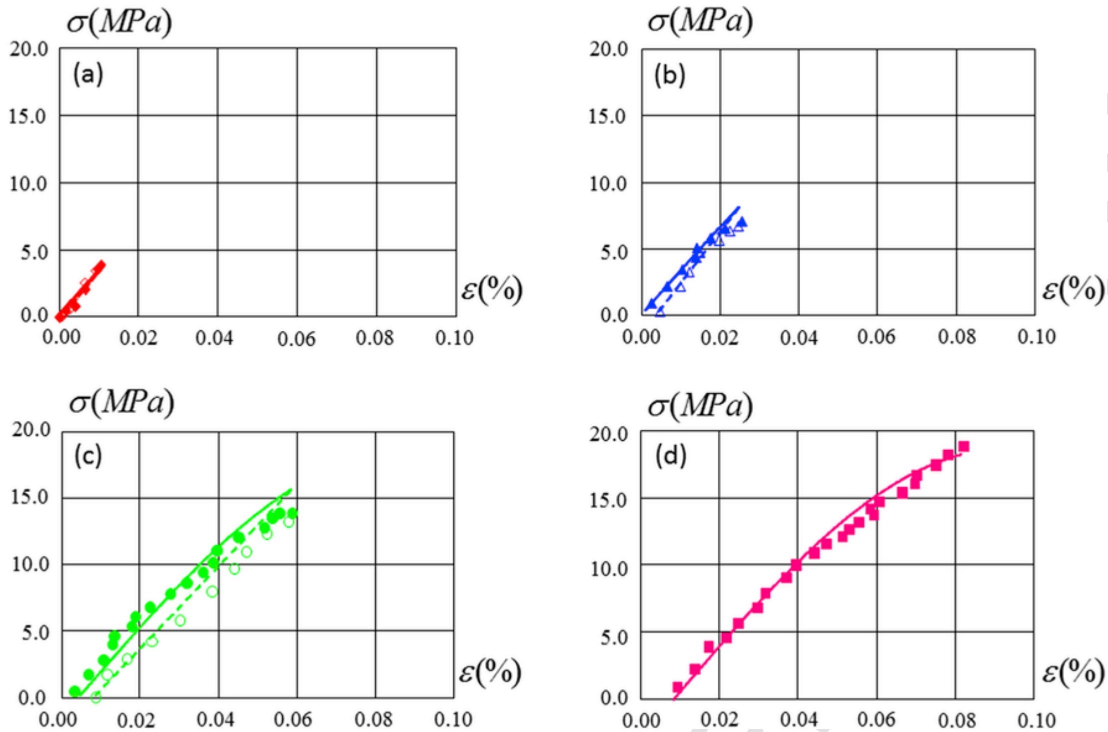

Fig. 10. Comparison of model predictions and experimental data for the three and a half loading-unloading cycles for MGS specimens.

UNCORRECTED PROOF

Note that the suggested micro-mechanism may not be the only one responsible for the observed stress-strain behavior. In particular, there is a possibility that, under tensile loading, certain branches of zig-zag-shaped cracks experience local compressive conditions and may undergo frictional sliding [5].

~~Remark.~~ We mention a peculiar detail of the stress-strain curves that seems to be observed in the data reported in Section 3: the unloading curve initially follows the loading one, starting to stiffen only after a certain amount of unloading - provided the peak load is sufficiently high. Fig. 11 gives a sketch that explains this feature in the framework of our model: at high peak loads, the opening displacement of cracks (at least, of many of them) is sufficiently large as to prevent immediate locking of the roughness profiles at unloading, so that the displacements of crack faces are not *initially* impeded, and the unloading curve closely follows the loading branch. At further unloading, cracks get locked by their asperities, and the material “stiffens”. This rather interesting feature can be observed in the measured stress-strain curves of Fig. 7a (or 9.c) at the third cycle, when the peak load goes above 75% of the rupture load (see inset in Fig. 11).

We also comment on the challenge of quantifying the crack density – that is encountered in many materials science applications. We emphasize that the “generalized crack density” – denoted by R – is introduced by necessity: although quantitative results exist for a number of non-circular shapes (see the book of Kachanov and Sevostianov [23]), the commonly used crack density parameter ρ is defined for the penny-shaped cracks only, whereas the actual crack geometries are quite “irregular” and do not resemble circles. At the same time, a certain measure of crack density *is* needed. In some specific cases, this difficulty can be solved [25]. However, in the context of our paper, it can be by-passed: it is not the crack density parameter itself that is needed, but its *evolution* with loading – and this aspect can be analyzed ~~bypassing~~ the explicit definition of the crack density parameter.

In Ref. [30], a direct comparison between the geometrical meaning of ρ and its determination via stress-strain curves has been attempted (using SEM images), but has yielded moderate agreement. The introduction of R would on one hand render such comparison impossible, but on the other hand would better correspond to the complicated microcrack shape, in spite of the fact that Kachanov and Sevostianov (2005) proved that moderate roughness would not undermine the geometrical meaning of ρ *under forward loading.*

The difficulty of a geometrical evaluation of the generalized crack density parameter R – or its increment under loading, ΔR - can be bypassed using cross-property connections [28,29]. This parameter can be determined in terms of the effective conductivity (thermal or electric) if these data are available. Indeed, the effective conductivity – in the framework of the differential scheme– is given by $k = k_0\, e^{-(8/9)\Delta\rho}$ in the case of circular cracks. As shown in Ref. [27], the concentration parameters for cracks of complex shapes are similar for the elasticity and conductivity problems, so that, similarly to Equation (2),

$$k = k_0\, e^{-\frac{8}{9}\Delta R} \tag{4}$$

Thus, the conductivity data determine~~s~~ the *value* of R - although its *geometrical* meaning may not be obvious. Further, the entire dependence $E = E(\varepsilon)$ can be determined in terms of the conductivity dependence $k = k(\varepsilon)$, using the explicit cross-property connection [28,29]. For microcracked materials, this connection – in the framework of the differential scheme applied to both the elastic and the

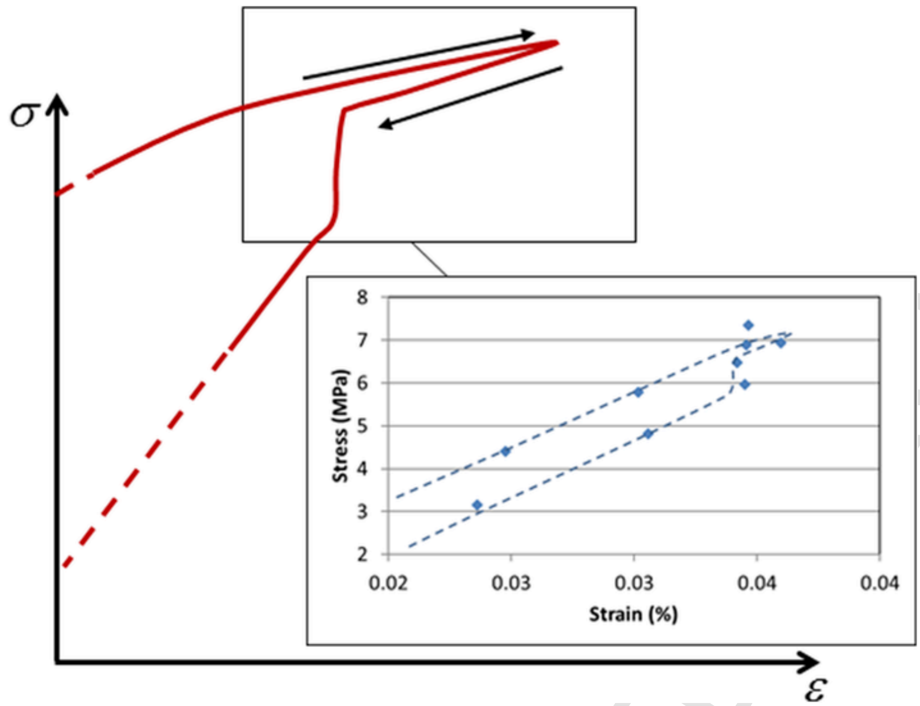

Fig. 11. Sketch that explains why unloading from a sufficiently high peak load initially follows the loading path (starting to stiffen only at later stages of unloading). The inset shows a part of the experimental data of Fig. 3a.

conductive properties – has the form

$$\frac{E}{E_0} = \left(\frac{k}{k_0}\right)^{9D_0/8} \tag{5}$$

We note, in conclusion, that the constructed model can be utilized to design for a specific non-linear tensile behavior of brittle microcracked polycrystalline materials.

Copyright notice

This manuscript has been authored by UT-Battelle, LLC under Contract No. DE-AC05-00OR22725 with the U.S. Department of Energy. The United States Government retains and the publisher, by accepting the article for publication, acknowledges that the United States Government retains a non-exclusive, paid-up, irrevocable, world-wide license to publish or reproduce the published form of this manuscript, or allow others to do so, for United States Government purposes. The Department of Energy will provide public access to these results of federally sponsored research in accordance with the DOE Public Access Plan (http://energy.gov/downloads/doe-public-access-plan).

Acknowledgments

Ryan Cooper is acknowledged for experimental assistance. I. Sevostianov and G. Bruno acknowledge financial support from DFG project BR 5199/3-1; M. Kachanov acknowledges support of the grant 14.Z50.31.0036 awarded to R. E. Alexeev Nizhny Novgorod Technical University by Department of Education and Science of the Russian Federation. A. Shyam thanks the following sponsors for funding (i) U.S. Department of Energy, Assistant Secretary for Energy Efficiency and Renewable Energy, Office of Vehicle Technologies, as part of the Propulsion Materials Program and (ii) U.S Department of Energy, Office of Fossil Energy, Solid State Energy Conversion Alliance (SECA) Program.

References

[1] G. Bruno, A.M. Efremov, B.R. Wheaton, J.E.Webb- Microcrack orientation in porous aluminum titanate, Acta Mater. 58 (2010) 6649–6655.
[2] G. Bruno, A.M. Efremov, C.P. An, B.R. Wheaton, D.J. Hughes, Connecting the macro and micro strain responses in technical porous ceramics. Part II microcracking, J. Mater. Sci. 47 (2012) 3674–3689.
[3] A. Shyam, E. Lara-Curzio, A. Pandey, T.R. Watkins, K.L. More, The thermal expansion, elastic and fracture properties of porous cordierite at elevated temperatures, J. Am. Ceram. Soc. 95 (2012) 1682–1691.
[4] S. Okubo, K. Fukui, Complete stress-strain curves for various rock types in uniaxial tension, Int. J. Rock Mech. Min. Sci. Geomech. Abstr. 33 (1996) 549–556.
[5] Z. Gao, J.W. Zimmerman, M. Kachanov, On microstructural mechanisms causing non-linear stress-strain behavior of porous ceramics under tension, Int. J. Fract. 183 (2013) 283–288.
[6] B.R. Müller, R.C. Cooper, A. Lange, A. Kupsch, M. Wheeler, M.P. Hentschel, A. Staude, A. Pandey, A. Shyam, G. Bruno, Stress-induced microcrack density evolution in β-eucryptite ceramics: experimental observations and possible route to strain hardening, Acta Mater. 144 (2018) 627–641.
[7] I. Hawkes, M. Mellor, Uniaxial testing in rock mechanics laboratories, Eng. Geol. 4 (1973) 177–285.
[8] B. Stimpson, R. Chen, Measurement of rock elastic moduli in tension and in compression and its practical significance, Can. Geotech. J. 30 (1993) 338–347.
[9] G. Young, Z. Cai, X. Zhang, D. Fu, An experimental investigation on the damage of granite under uniaxial tension by using a digital image correlation method, Optic Laser. Eng. 73 (2015) 46–52.
[10] R.C. Cooper, G. Bruno, M.R. Wheeler, A. Pandey, T.R. Watkins, A. Shyam, Effect of microcracking on the uniaxial tensile response of β-eucryptite ceramics: experiments and constitutive model, Acta Mater. 135 (2017) 361–371.
[11] F. Kroupa, Nonlinear behavior in compression and tension of thermally sprayed ceramic coatings, J. Therm. Spray Technol. 16 (1995) 84–95.
[12] T. Sadowski, S. Samborski, On the different behaviour of porous ceramic poly crystalline materials under tension and compression stress state, in: K.J. Bathe (Ed.), Computational Fluid and Solid Mechanics, Elsevier Science, 2003, pp. 615–618.

UNCORRECTED PROOF

[13] A. Pandey, A. Shyam, T.R. Watkins, E. Lara-Curzio, R.J. Stafford, K.J. Hemker, The uniaxial tensile response of porous and microcracked ceramic materials, J. Am. Ceram. Soc. 97 (3) (2014) 899–906.
[14] E.H. Saenger, O.S. Krueger, S.A. Shapiro, Effective elastic properties of fractured rocks: dynamic vs. static considerations, Int. J. Fract. 139 (2006) 569–576.
[15] D.A.G. Bruggeman, Berechnung verschiedener physikalisher Konstanten von heterogenen Substanzen. I. Dielectrizitätkonstanten und Leitfähigkeiten der Mischkörper aus isotropen Substanzen, Ann Physik Leipzig 24 (1935) 636–679.
[16] D.A.G. Bruggeman, Berechnung verschiedener physikalisher Konstanten von heterogenen Substanzen. III. Die elastische Konstanten der Quaiisotropen Mischkörper aus isotropen Substanzen, Ann Physik Leipzig 29 (1937) 160–178.
[17] A.S. Vavakin, R.L. Salganik, Effective characteristics of nonhomogeneous media with isolated inhomogeneities, Mech. Solid. 10 (1975) 65–75, (English transl. of Izvestia AN SSSR, Mekhanika Tverdogo Tela).
[18] Z. Hashin, The differential scheme and its application to cracked materials, J. Mech. Phys. Solid. 36 (1988) 719–734.
[19] R. McLaughlin, A study of the differential scheme for composite materials, Int. J. Eng. Sci. 15 (1977) 237–244.
[20] R.W. Zimmerman, The effect of microcracks on the elastic moduli of brittle materials, J. Mater. Sci. Lett. 4 (1985) 1457–1460.
[21] R.W. Zimmerman, Elastic moduli of solid containing spherical inclusions, Mech. Mater. 12 (1991) 17–24.
[22] I. Sevostianov, J. Kováčik, F. Simančík, Elastic and electric properties of closed-cell aluminum foams, Cross-property connection Materials Science and Engineering **A-420** (2006) 87–99.
[23] M. Kachanov, I. Sevostianov, Micromechanics of Materials, with Applications, Springer, 2018.
[24] Y. Gueguen, M. Kachanov, Effective elastic properties of cracked rocks – an overview, in: Y.M. Leroy, F.K. Lehner (Eds.), Mechanics of Crustal Rocks, Springer, 2011, pp. 65–108.
[25] M. Mear, I. Sevostianov, M. Kachanov, Elastic compliances of non-flat cracks, Int. J. Solid Struct. 44 (2007) 6412–6427.
[26] G. Bruno, O.V. Garlea, J. Muth, A.M. Efremov, T.R. Watkins, A. Shyam, Microstrain temperature evolution in β-eucryptite ceramics: measurement and model, Acta Mater. 60 (2012) 4982–4996.
[27] M. Kachanov, J. Rungamornrat, M. Mear, I. Sevostianov, Resistances of non-flat cracks and their relation to crack compliances, Int. J. Eng. Sci. 47 (2009) 754–766.
[28] I. Sevostianov, M. Kachanov, Explicit cross-property correlations for anisotropic two-phase composite materials, J. Mech. Phys. Solid. 50 (2002) 253–282.
[29] I. Sevostianov, M. Kachanov, Connections between elastic and conductive properties of heterogeneous materials, In: E. van der Giessen, H. Aref (Eds.), Advances in Applied Mechanics, vol. 42, Academic Press, 2009, pp. 69–252.
[30] G. Bruno, M. Kachanov, Porous microcracked ceramics under compression: micromechanical model of non-linear behavior, J. Eur. Ceram. Soc. 33 (2013) 2073–2085.
[31] A. Kožušníková, P. Konecny, E. Plevovaa, L. Králováa, Changes of physical properties of silesian granite due to heat loading, Procedia Engineering 191 (2017) 426–433.
[32] M.J. Heap, S. Vinciguerra, P.G. Meredith, The evolution of elastic moduli with increasing crack damage during cyclic stressing of a basalt from Mt. Etna volcano, Tectonophysics 471 (2009) 153–160.
[33] G. Bruno, A.M. Efremov, B.R. Wheaton, I. Bobrikov, V.G. Simkin, S. Misture, Micro and macroscopic expansion of stabilized porous aluminium titanate, J. Eur. Ceram. Soc. 30 (2010) 2555–2562.

UNCORRECTED PROOF